

A Rydberg Quantum Simulator

Hendrik Weimer,¹ Markus Müller,² Igor Lesanovsky,^{2,3} Peter Zoller,² and Hans Peter Büchler¹

¹*Institute for Theoretical Physics III, Universität Stuttgart, 70550 Stuttgart, Germany*

²*Institute for Theoretical Physics, University of Innsbruck,*

and Institute for Quantum Optics and Quantum Information of the Austrian Academy of Sciences, A-6020 Innsbruck, Austria

³*School of Physics and Astronomy, The University of Nottingham, Nottingham NG7 2RD, United Kingdom*

(Dated: April 11, 2012)

Following Feynman and as elaborated on by Lloyd, a universal quantum simulator (QS) is a controlled quantum device which reproduces the dynamics of any other many particle quantum system with short range interactions. This dynamics can refer to both coherent Hamiltonian and dissipative open system evolution. Here we show that laser excited Rydberg atoms in large spacing optical or magnetic lattices provide an efficient implementation of a universal QS for spin models involving (*high order*) *n*-body interactions. This includes the simulation of Hamiltonians of exotic spin models involving *n*-particle constraints such as the Kitaev toric code, color code, and lattice gauge theories with spin liquid phases. In addition, it provides the ingredients for dissipative preparation of entangled states based on engineering *n*-particle reservoir couplings. The key basic building blocks of our architecture are efficient and high-fidelity *n*-qubit entangling gates via auxiliary Rydberg atoms, including a possible dissipative time step via optical pumping. This allows to mimic the time evolution of the system by a sequence of fast, parallel and high-fidelity *n*-particle coherent and dissipative Rydberg gates.

Laser excited Rydberg atoms [1–7] stored in large spacing optical lattices [8] or magnetic trap arrays [9] offer unique possibilities for implementing scalable quantum information processors. In such a setup single atoms can be loaded and kept effectively frozen at each lattice site, with long-lived atomic ground states representing qubits or effective spin degrees of freedom. Lattice spacings of the order of a few μm allow *single site addressing* with laser light, and thus individual manipulation and readout of atomic spins. Exciting atoms with lasers to high-lying Rydberg states and exploiting the strong and long-range dipole-dipole or Van der Waals interactions between Rydberg states provides fast and *addressable 2-qubit entangling operations* or effective spin-spin interactions; recent theoretical proposals have extended Rydberg-based protocols towards a single step, high-fidelity entanglement of a mesoscopic number of atoms [10, 11]. Remarkably, the basic building blocks behind such a setup have been demonstrated recently in the laboratory by several groups [12, 13].

Motivated by and building on these new experimental

possibilities, we discuss below a Rydberg QS for many body spin models. As a key ingredient of our setup (see Fig. 1) we introduce additional auxiliary qubit atoms in the lattice, which play a two-fold role: First, they control and *mediate effective n-body spin interactions* among a subset of *n* system spins residing in their neighborhood in the lattice. In our scheme this is achieved efficiently making use of single-site addressability and a parallelized multi-qubit gate, which is based on a combination of strong and long-range Rydberg interactions and electromagnetically induced transparency (EIT), as suggested recently in Ref. [11]. Second, the auxiliary atoms can be optically pumped, thereby providing a dissipative element, which in combination with Rydberg interactions results in *effective collective dissipative dynamics* of a set of spins located in the vicinity of the auxiliary particle, which itself eventually factors out from the system spin dynamics. The resulting coherent and dissipative dynamics on the lattice can be represented by, and thus simulates a master equation $\dot{\rho} = -(i/\hbar)[H, \rho] + \mathcal{L}\rho$ [14], where the Hamiltonian $H = \sum_{\alpha} H_{\alpha}$ is the sum of *n*-body interaction terms, involving a quasi-local collection of spins in the lattice. The Liouvillian term $\mathcal{L} = \sum_{\beta} \mathcal{D}(c_{\beta})$ with $\mathcal{D}(c)\rho = c\rho c^{\dagger} - \frac{1}{2}c^{\dagger}c\rho - \rho\frac{1}{2}c^{\dagger}c$ in Lindblad form governs the dissipative time evolution, where the many-particle quantum jump operators c_{β} involve products of spin operators in a given neighborhood.

The actual dynamics of our system is performed as a stroboscopic sequence of coherent and dissipative operations involving the auxiliary Rydberg atoms over time steps τ , with the master equation emerging as a coarse grained description of the time evolution. For purely coherent dynamics governed by the Hamiltonian, this is the familiar “digital QS” [15, 16] where for each time step the evolution operator is implemented via a Trotter expansion $e^{-iH\tau/\hbar} \approx \prod_{\alpha} e^{-iH_{\alpha}\tau/\hbar}$ and a certain error associated with the non-commutativity of the quasi-local interactions H_{α} . The concept of stroboscopic time evolution is readily adapted to the dissipative case by interspersing coherent propagation and dissipative time steps $e^{\mathcal{L}\tau} \approx \prod_{\beta} e^{\mathcal{D}(c_{\beta})\tau}$, providing an overall simulation of the master equation by sweeping over the whole lattice with our coherent and dissipative operations. Many of these steps can in principle be done in a highly parallel way, rendering the time for a simulation step independent on the system size. In our scheme the characteristic energy

scale of the many-body interaction terms is essentially the same for two-body, four- or higher-order interaction terms, and mainly limited by the fast time-scale to perform the parallel mesoscopic Rydberg gate operations.

COHERENT AND DISSIPATIVE MANY BODY SPIN DYNAMICS

Before proceeding with the concrete physical implementation of our Rydberg QS, we find it convenient to discuss special spin models and master equations of interest, starting with an explicit example: Kitaev’s toric code. We will discuss the realization of a more complex setup of a three-dimensional $U(1)$ lattice gauge theory giving rise to a spin liquid phase in the last section.

Kitaev’s *toric code* is a paradigmatic, exactly solvable model, out of a large class of spin models, which have recently attracted a lot of interest in the context of studies on topological order and quantum computation. It considers a two-dimensional setup, where the spins are located on the edges of a square lattice [17]. The Hamiltonian $H = -E_0 \left(\sum_p A_p + \sum_s B_s \right)$ is a sum of mutually commuting stabilizer operators $A_p = \prod_{i \in p} \sigma_i^x$ and $B_s = \prod_{i \in s} \sigma_i^z$, which describe *four-body interactions* between spins located around plaquettes (A_p) and vertices (B_s) of the square lattice (see Fig. 1b). The ground state of the Hamiltonian is a simultaneous eigenstates of all stabilizer operators A_p and B_s with eigenvalues $+1$, and gives rise to a topological phase: the ground state degeneracy depends on the boundary conditions and topology of the setup, and the elementary excitation exhibit anyonic statistics under braiding. The toric code shows two types of excitations corresponding to -1 eigenstates of each stabilizer A_p (“magnetic charge”) and B_p (“electric charge”).

A dissipative dynamics which “cools” into the ground state manifold is provided by a Liouvillian with quantum jump operators,

$$c_p = \frac{1}{2} \sigma_i^z [1 - A_p], \quad c_s = \frac{1}{2} \sigma_j^x [1 - B_s], \quad (1)$$

with $i \in p$ and $j \in s$, which act on four spins located around plaquettes p and vertices s , respectively. The jump operators are readily understood as operators which “pump” from -1 into $+1$ eigenstates of the stabilizer operators: the part $(1 - A_p)/2$ is a projector onto the eigenspace of A_p with -1 eigenvalue, while all states in the $+1$ eigenspace are dark states. The subsequent spin flip σ_j^x transfers the excitation to the neighboring plaquette. The jump operators then give rise to a random walk of anyonic excitations on the lattice, and whenever two excitations of the same type meet they are annihilated, resulting in a cooling process, see Fig. 2. Similar arguments apply to c_s . Efficient cooling is achieved by alternating the index i of the spin, which is flipped.

Our choice of the jump operator follows the idea of reservoir engineering of interacting many-body systems as discussed in Ref. [18, 19]. In contrast to alternative schemes for measurement based state preparation [20], here, the cooling is part of the time evolution of the system. These ideas can be readily generalized to more complex stabilizer states and to setups in higher dimensions, as in, e.g., the color code (see Fig. 1c) [21]. As a final remark we would like to mention that the toric code can also be derived as a perturbative limit of a Hamiltonian with two-body interactions on a honeycomb lattice [22], of which implementations have been suggested both for cold atoms [23] and condensed matter systems [24]. In our approach the higher-order interactions arise in a non-perturbative way and the scheme also allows for dissipative state preparation.

IMPLEMENTATION OF A SINGLE TIME STEP

We now turn to the physical implementation of the digital quantum simulation. The system and auxiliary atoms are stored in a deep optical lattice or magnetic trap arrays with one atom per lattice site, where the motion of the atoms is frozen and the remaining degree of freedom of the system and auxiliary atoms are effective spin- $1/2$ systems described by the two long-lived ground states $|A\rangle_i$ and $|B\rangle_i$ and $|0\rangle_c$ and $|1\rangle_c$, respectively (see Fig. 1a). We first discuss the elements of the digital QS for a small local setup, and present the extension to the macroscopic lattice system below. To be specific, we will focus on a single plaquette in the example of Kitaev’s toric code outlined above.

The implementation of the four-body spin interaction $A_p = \prod_i \sigma_i^x$ and the jump operator c_p uses an auxiliary qubit located at the centre of the plaquette (see Fig.1b). The general approach then consists of three steps (see Fig. 3b): (i) We first perform a gate sequence G which encodes the information whether the four spins are in a $+1$ or -1 eigenstate of A_p in the two internal states of the auxiliary atom. (ii) In a second step, we apply gate operations, which depend on the internal state of the control qubit. Due to the previous mapping these manipulations of the control qubit are equivalent to manipulations on the subspaces with fixed eigenvalues of A_p . (iii) Finally, the mapping G is reversed, and the control qubit is re-initialized incoherently in its internal state $|0\rangle$ by optical pumping.

The mapping G is a sequence of three gate operations

$$G = U_c(\pi/2)^{-1} U_g U_c(\pi/2), \quad (2)$$

where $U_c(\pi/2) = \exp(-i\pi\sigma_y/4)$ is a standard $\pi/2$ -single qubit rotation of the control qubit and the parallelized many-body Rydberg gate [11] takes the form (see Fig. 1a for the required electronic level scheme and the Methods

section for a brief summary)

$$U_g = |0\rangle\langle 0|_c \otimes \mathbf{1} + |1\rangle\langle 1|_c \otimes \prod_{i \in P} \sigma_i^x. \quad (3)$$

For the control qubit initially prepared in $|0\rangle_c$, the gate G coherently transfers the control qubit into the state $|1\rangle_c$ ($|0\rangle_c$) for any system state $|\lambda, -\rangle$ ($|\lambda, +\rangle$), with $|\lambda, \pm\rangle$ denoting the eigenstates of A_p , i.e., $A_p|\lambda, \pm\rangle = \pm|\lambda, \pm\rangle$, see Fig. 3.

For the *coherent time evolution*, the application of a phase shift $\exp(i\phi\sigma_c^z)$ on the control qubit and the subsequent reversion of the gate, G^{-1} , implements the time evolution according to the many-body interaction A_p , i.e.,

$$U_{\text{int}} = \exp(i\phi A_p) = G^{-1} \exp(i\phi\sigma_c^z) G. \quad (4)$$

The control qubit returns to its initial state $|0\rangle_c$ after the complete sequence and therefore effectively factors out from the dynamics of the system spins. For small phase imprints $\phi \ll 1$, the mapping reduces to the standard equation for coherent time evolution

$$\partial_t \rho = -\frac{i}{\hbar} E_0 [-A_p, \rho] + o(\phi^2). \quad (5)$$

The energy scale for the four-body interaction A_p becomes $E_0 = \hbar\phi/\tau$ with τ the time required for the implementation of a single time step.

On the other hand, for the *dissipative dynamics*, we are interested in implementing the jump operator c_p (see Eq. 1). To this purpose, after the mapping G , we apply a controlled spin flip onto one of the four system spins,

$$U_{z,i}(\theta) = |0\rangle\langle 0|_c \otimes \mathbf{1} + |1\rangle\langle 1|_c \otimes \Sigma \quad (6)$$

with $\Sigma = \exp(i\theta\sigma_i^z)$. As desired, the sequence $G^{-1}U_{z,i}(\theta)G$ leaves the low energy sector $|\lambda, +\rangle$ invariant since these states are mapped onto $|0\rangle_c$ and are therefore unaffected by $U_{z,i}(\theta)$. In contrast - with a certain probability - the sequence performs a controlled spin flip on the states $|\lambda, -\rangle$. Once a spin is flipped, the auxiliary qubit remains in the state $|1\rangle_c$, and optical pumping from $|1\rangle_c$ to $|0\rangle_c$ is required to re-initialize the system, guaranteeing that the control qubit again factors out from the system dynamics. The optical pumping constitutes the dissipative element in the system and allows one to remove entropy in order to cool the system. Note that while optical pumping may lead to heating of the motional degrees of freedom, it is possible to recool the control atom afterwards, e.g., by sideband cooling. The two qubit gate $U_{z,i}(\theta)$ is implemented in close analogy to the many-body Rydberg gate U_g previously discussed. For small phases θ the operator Σ can be expanded, and the density matrix ρ of the spin system evolves in one dissipative time step according to the Lindblad form

$$\partial_t \rho = \kappa \left[c_p \rho c_p^\dagger - \frac{1}{2} \{ c_p^\dagger c_p \rho + \rho c_p^\dagger c_p \} \right] + o(\theta^3) \quad (7)$$

with the jump operators c_p given in Eq. (1) and the cooling rate $\kappa = \theta^2/\tau$. Note, that the cooling also works for large phases θ , and therefore the most efficient dissipative state preparation is achieved with $\theta = \pi$.

The above scheme for the implementation of the many-body interaction A_p and the dissipative cooling with c_p can be naturally extended to arbitrary many-body interactions between the system spins surrounding the control atom, as e.g., the B_p interaction terms in the above toric code. Gate operations on single system spins allow to transform σ_i^x in σ_i^y and σ_i^z , in accordance with previous proposals for digital simulation of spin Hamiltonians [25], while selecting only certain spins to participate in the many-body gate via local addressability gives rise to the identity operator for the non-participating spins. Consequently, we immediately obtain the implementation of the general many-body interaction and jump operators

$$A_\alpha = \prod_i W_i, \quad c_\beta = \frac{1}{2} Q_i \left[1 - \prod_j W_j \right] \quad (8)$$

with $W_i, Q_i \in \{1, \sigma_i^x, \sigma_i^y, \sigma_i^z\}$. Here, α and β stand for a collection of indices characterizing the position of the local interaction and the interaction type. Note that A_α also includes single particle terms, as well as two-body interactions.

TOOLBOX FOR DIGITAL QUANTUM SIMULATION

Extending the analysis to a *large lattice system* with different, possibly non-commuting interaction terms in the Hamiltonian, i.e., $H = \sum_\alpha E_\alpha A_\alpha$ and dissipative dynamics described by a set of jump operators c_β with damping rates κ_β , provides a complete toolbox for the quantum simulation of many-body systems. Each term is characterized by a phase ϕ_α (θ_β) written during a single time step determining its coupling energy $E_\alpha = \hbar\phi_\alpha/\tau$ and damping rate $\kappa_\beta = \theta_\beta^2/\tau$. For small phases $\phi_\alpha \ll 1$ and $\theta_\beta^2 \ll 1$, the sequential application of the gate operations for all interaction and damping terms reduces to the master equation of Lindblad form,

$$\partial_t \rho = -\frac{i}{\hbar} [H, \rho] + \sum_\beta \kappa_\beta \left[c_\beta \rho c_\beta^\dagger - \frac{1}{2} (c_\beta^\dagger c_\beta \rho + \rho c_\beta^\dagger c_\beta) \right]. \quad (9)$$

The choice of the different phases during each time step allows for the control of the relative interaction strength of the different terms, as well as the simulation of inhomogeneous and time dependent systems.

The characteristic energy scale for the interactions E_α and damping rates κ_β are determined by the ratio between the time scale τ required to perform a single time step, and the phase difference ϕ_α and θ_β written during

these time steps. It is important to stress that within our setup, the interactions are quasi-local and only influence the spins surrounding the control qubit. Consequently, the lattice system can be divided into a set of sublattices on which all gate operations that are needed for a single time step τ , can be carried out in parallel. Then, the time scale for a single step τ becomes independent on the system size and is determined by the product of the number z of such sublattices and the duration τ_s of all gate operations on one sublattice. In our setup, τ_s is mainly limited by the duration of the many-body Rydberg gate U_g , which is on the order of $\sim 1\mu\text{s}$ (see Methods section for details). For the toric code discussed above, we have to apply the many-body gate twice for every interaction term (see Fig. 3), and with $z = 4$, we obtain $\tau \sim$ a few μs , resulting in characteristic energy scales and cooling rates of the order of hundred kHz. For the simulation of Hamiltonian dynamics this energy scale may be somewhat lower if Trotterization errors have to be taken care of. It is a crucial aspect of this quantum simulation with Rydberg atoms that it can be performed fast and is compatible with current experimental time scales of cold atomic gases [26].

Finally, we would like to point out that imperfect gate operations provide in leading order small perturbations for the Hamiltonian dynamics and weak dissipative terms; see Methods section and Fig. 2 for a numerical analysis of the induced errors. However, the thermodynamic properties and dynamical behaviour of a strongly interacting many-body system are in general robust to small perturbations in the Hamiltonian; e.g., the stability of the toric code for small magnetic fields has recently been demonstrated [27]. Consequently, small imperfections in the implementation of the gate operations are tolerable.

An important aspect for the characterization of the final state is the measurement of correlation functions $\chi = \langle A_{\alpha_1} \dots A_{\alpha_n} \rangle$, where A_{α_j} denote local, mutually commuting many-body observables. In our scheme, the observables A_{α_j} can be measured via the mapping G of the system information onto auxiliary qubits and their subsequent state selective detection. In analogy to noise correlation measurements in cold atomic gases [28, 29] the repeated measurement via such a detection scheme provides the full distribution function for the observables, and therefore allows to determine the correlation function χ in the system. Consequently, in the above discussion of Kitaev's toric code, the necessary string operators characterizing topological order can be detected.

LATTICE GAUGE THEORY

In the first example, we discussed the implementation of the quantum simulator for the toric code, and the extension to more complex stabilizer states is straightfor-

ward. In the following, we will show that our approach can also be extended to systems with non-commuting terms in the Hamiltonian. As an example, we focus on a three-dimensional $U(1)$ -lattice gauge theory [30], and show that dissipative ground state cooling can also be achieved in such complex models. Such models have attracted a lot of recent interest in the search for 'exotic' phases and spin liquids [31–34]. The three-dimensional setup consists of spins located on the links of a cubic lattice (see Fig. 1d). The lattice structure for the spins can be viewed as a corner sharing lattice of octahedra with one site of the cubic lattice in the center of each octahedron. The Hamiltonian for the $U(1)$ lattice gauge theory takes the form

$$H = U \sum_o (S_o^z)^2 - J \sum_p B_p + V N_{\text{RK}}, \quad (10)$$

where the first term in the Hamiltonian defines a low energy sector consisting of allowed spin configuration with an equal number of up and down spins on each octahedron, i.e., spin configurations with vanishing total spin $S_o^z = \sum_{i \in o} \sigma_i^z$ on each octahedron. The second term denotes a ring exchange interaction on each plaquette with $B_p = S_1^+ S_2^- S_3^+ S_4^- + S_1^- S_2^+ S_3^- S_4^+$; here $S_i^\pm = [\sigma_i^x \pm i\sigma_i^y]/2$ and the numbering is clockwise around the plaquette. This term flips a state with alternating up and down spins on a plaquette, i.e., $|\uparrow, \downarrow, \uparrow, \downarrow\rangle_p \rightarrow |\downarrow, \uparrow, \downarrow, \uparrow\rangle_p$. The last term denotes the so-called Rokhsar-Kivelson term, which counts the total number of flipable plaquettes $N_{\text{RK}} = \sum_p B_p^2$. While the ring exchange interaction commutes with the spin constraint, ring exchange terms on neighboring plaquettes are non-commuting. At the Rokhsar-Kivelson point with $J = V$, the system becomes exactly solvable [35], and it has been proposed that in the regime $0 \leq V \leq J$ the ground state is determined by a spin liquid smoothly connected to the Rokhsar-Kivelson point [33]: the properties of this spin liquid are given by an artificial 'photon' mode, gapped excitations carrying an 'electric' charge (violation of the constraint on an octahedron), which interact with a $1/r$ Coulomb potential mediated by the artificial photons, and gapped magnetic monopoles.

In the following, we present the implementation of this Hamiltonian within our scheme for the digital quantum simulation and demonstrate that dissipative ground state cooling can be achieved at the Rokhsar-Kivelson point. The control qubits reside in the center of each octahedron (on the lattice sites of the 3D cubic lattice) controlling the interaction on each octahedron, and in the center of each plaquette for the ring exchange interaction B_p , see Fig. 1. Then, the coherent time evolution of the Hamiltonian (10) can be implemented in analogy to the above discussion by noting that the ring exchange interaction B_p and N_{RK} can be written as a sum of four-body interactions of the form (8), while the constraint on the octahedra is an Ising interaction, see Methods section.

Next, we discuss the jump operators for the dissipative ground state preparation. The cooling into the subspace with an equal number of up and down spins on each octahedron is obtained by the jump operator

$$c_s = \frac{1}{4} \left[1 + \prod_j e^{-i\frac{\pi}{6}\sigma_j^z} \right] \sigma_i^x \left[1 - \prod_j e^{i\frac{\pi}{6}\sigma_j^z} \right], \quad (11)$$

where the product is carried out over the six spins located on the corners of the octahedron (see Fig. 1d). The ‘interrogation’ part $1 - \prod_j \exp(i\frac{\pi}{6}\sigma_j^z)$ of the jump operator vanishes if applied to any state with three up and three down spins, while in all other cases a spin is flipped. Then the cooling follows in analogy to the cooling in the toric code by the diffusion of the ‘electric’ charges. Identifying each spin up with a ‘dimer’ on the link, all states satisfying the constraints on the octahedra can be viewed as a dimer covering with three dimers meeting at each site of the cubic lattice, see Fig. 4a. Within this description, the ground state at the Rokhsar-Kivelson point is given by the condensation of the dimer coverings [34], i.e., the equal weight superposition of all dimer coverings. The condensation of the dimer coverings is then achieved by the jump operator

$$c_p = \frac{1}{2} \sigma_i^z [1 - B_p] B_p. \quad (12)$$

This jump operator has two dark states, which are the 0 and +1 eigenstates of B_p . The 0 eigenstate corresponds to a non-flippable plaquette, while the +1 eigenstate is the equal weight superposition of the original dimer covering and the dimer covering obtained by flipping the plaquette (i.e., the +1 eigenstate). Finally, the jump operator c_p transforms the third eigenstate with eigenvalue -1 into the +1 eigenstate. After acting on all plaquettes, the system is cooled into the dark state which is the equal superposition of all dimer coverings, which can be reached by flipping different plaquettes. The cooling of these jump operators is demonstrated via a numerical simulation for a small system of 4 unit cells, see Fig. 4b.

The implementation of the digital quantum simulations provides full control on the spatial and temporal interaction strengths. Therefore, there are two possibilities to analyze the phase diagram for arbitrary interaction strengths: (i) The possibility to vary the different coupling strengths in time allows us adiabatically explore the phase diagram; the adiabatic preparation using the Trotter expansion is shown in Fig. 4c. (ii) On the other hand, the spatial control of the coupling parameters allows us to divide the lattice into a system and a bath. The ground state of the bath is given by the Rokhsar-Kivelson state, which can be continuously cooled via the dissipative terms, while the system part is sympathetically cooled due to its contact with the bath; in analogy to the cooling well known in condensed matter systems.

METHODS

Gate errors

In the following, we discuss the influence of a gate error onto the dynamics of the system. For simplicity, we illustrate the general behaviour for an error in the many-body gate U_g for the coherent time evolution of the many-body interaction A_p . The imperfect many-body gate operation can be written

$$\tilde{U}_g = |0\rangle\langle 0|_c \otimes e^{i\phi Q} + |1\rangle\langle 1|_c \otimes A_p, \quad (13)$$

where the perfect gate U_g is recovered for $Q \rightarrow 0$ and the operator $Q = Q^\dagger$ acts on the system spins surrounding the control atom. This form of the error is motivated by the specific implementation of the gate [11]; however, it can be seen that different errors in the many-body and single particle gates will lead to similar phenomena. For the *coherent* time evolution, the imperfect gate gives rise to a finite amplitude for the control qubit to end up in the state $|1\rangle_c$. Consequently, optical pumping of the control qubit is required to reinitialize the system. Then the gate operations on a single plaquette give rise to the mapping of the density matrix onto

$$\rho \rightarrow C\rho C^\dagger + D\rho D^\dagger \quad (14)$$

with $(\Theta \equiv e^{i\phi Q})$

$$C = \frac{1}{2} [(\Theta^2 + \mathbf{1}) \cos \phi + (\Theta A_p + A_p \Theta) i \sin \phi] \quad (15)$$

$$\approx \exp[i\phi(A_p + Q)] - \frac{\phi^2}{2} Q^2 \quad (16)$$

$$D = \frac{1}{2} [(\Theta^2 - \mathbf{1}) \cos \phi + (\Theta A_p - A_p \Theta) i \sin \phi] \quad (17)$$

$$\approx -i\phi Q. \quad (18)$$

The last equations hold with an accuracy up to third order in the small parameter ϕ . Consequently, the optical pumping has no influence in leading order, and the system is well described by a Hamiltonian evolution with the modified Hamiltonian $H = -(\hbar/\tau)\phi[A_p + Q]$. The characteristic energy scale of the correction is again given by $\hbar\phi/\tau$, and consequently describes a small perturbation if $|Q| \ll 1$. In second order expansion in the small parameter ϕ , the mapping of the density matrix reduces to

$$\rho \rightarrow \rho - i\phi[h, \rho] - \frac{\phi^2}{2} [h, [h, \rho]] + \frac{\phi^2}{2} (2Q\rho Q - \{Q^2, \rho\}), \quad (19)$$

with $h = -[A_p + Q]$. The first terms on the right hand side describe the coherent evolution of the system with the evolution operator $\exp(-i\phi h)$ consistently expanded up to second order, while the last term takes the standard Lindblad form for a dissipative coupling with the jump operator $c_e = Q$ describing a dephasing with the rate $\kappa_e = \phi^2/\tau$.

Mesoscopic Rydberg gate

In the following we briefly summarise the main properties and requirements of the many-body Rydberg gate U_g introduced in Ref. [11]. The internal level structure of the control atom and the surrounding ensemble atoms is depicted in Fig. 1. The underlying physical mechanism of the gate operation (3) is a conditional Raman transfer of all ensemble atoms between their logical internal states $|A\rangle$ and $|B\rangle$, which - depending on the internal state $|0\rangle$ or $|1\rangle$ of the control qubit - is either inhibited or enabled. The gate is realised by the following three laser pulses: (i) A first state selective π -pulse acting on the control atom changes the ground state $|1\rangle$ into the Rydberg state $|r\rangle$. (ii) During the whole gate operation, a strong coupling laser of Rabi frequency Ω_c constantly acts on all ensemble atoms and off-resonantly couples the Rydberg level $|R\rangle$ to the intermediate level $|P\rangle$ with a detuning Δ . Its frequency is chosen such that it is in two-photon resonance with the two Raman laser beams of Rabi frequency Ω_p (see Fig. 1), thereby establishing a condition known as electromagnetically induced transparency (EIT) [36]. The system then adiabatically follows a zero energy dark state, which at the end of the pulse is identical to the one in the beginning. In consequence, when the Raman laser pulses are applied - and provided the control atom resides in state $|0\rangle$ - this two-photon resonance condition effectively blocks the Raman transfer from $|A\rangle$ to $|B\rangle$. In case the control atom was excited to the Rydberg state $|r\rangle$ in step (i), the large Rydberg-Rydberg interaction energy shift (dipole blockade) lifts the blocking condition for the ensemble atoms and thus the Raman transfer takes place. (iii) Finally, the control atom is transferred from state $|r\rangle$ back to $|1\rangle$ via a second π -pulse. The total time T_{gate} required for the gate is mainly limited by the duration of the Raman pulse, resulting in $T_{\text{gate}} \sim 16\pi\Delta/(3\Omega_p^2)$. The principal error source for the many-body gate is due to the Rydberg-Rydberg interactions between the ensemble atoms. For N ensemble atoms the accumulated phase errors scale like $\phi|Q| \sim N(N-1)(\Omega_p/\Omega_c)^2$, i.e., they depend on all possible pair combinations and the probability of an ensemble atom being excited to the Rydberg state due to non-adiabatic processes [11].

Experimental implementation

Our setup consists of control and ensemble atoms trapped in large spacing optical lattices (see Fig. 1), so that single site addressability can be achieved. In order to manipulate ensemble atoms independently, their spacing a must be larger than the wavelength λ_p of the Raman lasers for the many-body gate. Such a spatial resolution can be achieved by tightly focussing the laser beam, by employing superlattice beams for the gate pulses, or sub-wavelength addressing techniques based on magnetic

field gradients [37] or dark state resonances [38]. Control and ensemble atoms can be distinguished spectroscopically, e.g., by using different hyperfine states in two state-dependent lattices. A suitable set of parameters is determined by balancing the need for sufficiently large lattice spacing with at the same time strong Rydberg interactions for a fast and high-fidelity many-body gate.

We require the ensemble atoms to be separated by $a = 3.5\lambda_p \approx 1.5\mu\text{m}$ and a fast many-body gate with $T_{\text{gate}} = 1.5\mu\text{s}$ (which is much shorter than decoherence times, e.g., due to radiative decay of the Rydberg states). For ^{87}Rb this is achieved by choosing $\Omega_p = 2\pi \times 67\text{ MHz}$, $\Delta = 2\pi \times 2\text{ GHz}$, $\Omega_c = 2\pi \times 1\text{ GHz}$, an interaction strength of $V = 10\hbar\Omega_c^2/\Delta$, and using the Rydberg states $|r\rangle_c = |59s\rangle$ and $|R\rangle_i = |53s\rangle$, respectively. Note that for these Rydberg states the corresponding distances are still larger than the LeRoy radius, i.e., there is no overlap between the wavefunctions of the atoms. Furthermore, corrections to a pure van der Waals interaction due to resonant dipole-dipole couplings [39, 40] are also small, while using s states ensures the interaction being isotropic. For these parameters, the errors due to ensemble-ensemble interactions result for $N = 4$ atoms in $\phi|Q| = 0.2$.

Further errors arise from crosstalk between plaquettes being processed in parallel, i.e. when a control atom interacts with ensemble atoms of distant plaquettes. Due to the rapid decay of the van der Waals interaction the residual interaction is reduced by a factor of at least 125 on a square lattice. For $V = 10\hbar\Omega_c^2/\Delta$ the resulting error is of similar size as due to ensemble-ensemble interactions. This error can be further reduced by increasing the number of sublattices z such that only every second or third plaquette is processed in parallel.

Quantum gates for the $U(1)$ lattice gauge theory

The Hamiltonian giving rise to the constraint for the spins on the octahedra can be expressed as a sum of Ising interactions,

$$(S_o^z)^2 = \sum_{i \neq j}^6 \sigma_i^z \sigma_j^z + \text{const}, \quad (20)$$

which allow for an efficient implementation using the general toolbox for quantum simulation. The implementation for the jump operators for the constraint is obtained in analogy to the general jump operators with the many-body gate U_g replaced by the gate $|0\rangle\langle 0|_c \otimes \mathbf{1} + |1\rangle\langle 1|_c \otimes \prod_i \exp(i\frac{\pi}{6}\sigma_i^z)$. On the other hand, the ring exchange interaction can be written as a sum of commuting four-

body interactions

$$\begin{aligned}
B_p = & \frac{1}{8} \sum_{j=1}^8 B_p^{(j)} = \frac{1}{8} (\sigma_1^x \sigma_2^x \sigma_3^x \sigma_4^x + \sigma_1^y \sigma_2^y \sigma_3^y \sigma_4^y \\
& + \sigma_1^x \sigma_2^x \sigma_3^y \sigma_4^y + \sigma_1^y \sigma_2^y \sigma_3^x \sigma_4^x - \sigma_1^x \sigma_2^y \sigma_3^x \sigma_4^y \\
& - \sigma_1^y \sigma_2^x \sigma_3^y \sigma_4^x + \sigma_1^x \sigma_2^y \sigma_3^y \sigma_4^x + \sigma_1^y \sigma_2^x \sigma_3^x \sigma_4^y). \quad (21)
\end{aligned}$$

Likewise, the Rokhsar-Kivelson term can be decomposed into

$$\begin{aligned}
B_p^2 = & \frac{1}{8} \sum_{j=1}^8 N_p^{(j)} = \frac{1}{8} (\sigma_1^0 \sigma_2^0 \sigma_3^0 \sigma_4^0 - \sigma_1^0 \sigma_2^0 \sigma_3^z \sigma_4^z \\
& + \sigma_1^0 \sigma_2^z \sigma_3^0 \sigma_4^z - \sigma_1^0 \sigma_2^z \sigma_3^z \sigma_4^0 - \sigma_1^z \sigma_2^0 \sigma_3^0 \sigma_4^z \\
& + \sigma_1^z \sigma_2^0 \sigma_3^z \sigma_4^0 - \sigma_1^z \sigma_2^z \sigma_3^0 \sigma_4^0 + \sigma_1^z \sigma_2^z \sigma_3^z \sigma_4^z), \quad (22)
\end{aligned}$$

where σ_i^0 is the identity matrix. Consequently, the coherent time evolution follows again from the general toolbox, while the jump operators for cooling into the ground state at the Rokhsar-Kivelson point effectively cool into the zero eigenvalue eigenstate of the operators

$$\frac{1}{2} [1 - B_p] B_p = \frac{1}{16} \sum_{j=1}^{16} C_p^{(j)} = \frac{1}{16} \left[\sum_{j=1}^8 B_p^{(j)} - \sum_{j=1}^8 N_p^{(j)} \right]. \quad (23)$$

This can be achieved by replacing the gate U_g with

$$\begin{aligned}
U_B = & |0\rangle\langle 0|_c \otimes \mathbf{1} + |1\rangle\langle 1|_c \otimes \exp \left[i \frac{\pi}{2} (1 - B_p) B_p \right] \\
= & \prod_{j=1}^{16} U_c(\pi/2)^{-1} U_j U_c(\pi/2) \exp(i\pi/32\sigma_c^z) \\
& U_c(\pi/2)^{-1} U_j U_c(\pi/2), \quad (24)
\end{aligned}$$

with $U_j = |0\rangle\langle 0|_c \otimes \mathbf{1} + |1\rangle\langle 1|_c \otimes C_p^{(j)}$. This gate operation leaves states with eigenvalue 0, +1 of B_p invariant, while the -1 eigenvalue picks up a phase of π . It can be implemented as a product of many-body gates which derive directly from the standard gate U_g with the combination of spin rotations.

Acknowledgments

This work was supported by the Austrian Science Foundation (FWF), and by the Deutsche Forschungsgemeinschaft (DFG) within SFB/TRR 21.

Author contributions

All five authors contributed equally to all parts of this work.

Author information

Reprints and permissions information is available online at <http://npg.nature.com/reprintsandpermissions>. Correspondence and requests for materials should be addressed to H.W.

-
- [1] Gallagher, T. F. *Rydberg Atoms* (Cambridge University Press, Cambridge, 1994).
 - [2] Tong, D. *et al.* Local Blockade of Rydberg Excitation in an Ultracold Gas. *Phys. Rev. Lett.* **93**, 063001 (2004).
 - [3] Singer, K., Reetz-Lamour, M., Amthor, T., Marcassa, L. G. & Weidemüller, M. Suppression of Excitation and Spectral Broadening Induced by Interactions in a Cold Gas of Rydberg Atoms. *Phys. Rev. Lett.* **93**, 163001 (2004).
 - [4] Cubel, T. *et al.* Coherent population transfer of ground-state atoms into Rydberg states. *Phys. Rev. A* **72**, 023405 (2005).
 - [5] Vogt, T. *et al.* Dipole Blockade at Förster Resonances in High Resolution Laser Excitation of Rydberg States of Cesium Atoms. *Phys. Rev. Lett.* **97**, 083003 (2006).
 - [6] Mohapatra, A. K., Jackson, T. R. & Adams, C. S. Coherent Optical Detection of Highly Excited Rydberg States Using Electromagnetically Induced Transparency. *Phys. Rev. Lett.* **98**, 113003 (2007).
 - [7] Heidemann, R. *et al.* Evidence for coherent collective Rydberg excitation in the strong blockade regime. *Phys. Rev. Lett.* **99**, 163601 (2007).
 - [8] Nelson, K. D., Li, X. & Weiss, D. S. Imaging single atoms in a three dimensional array. *Nature Phys.* **3**, 556–560 (2007).
 - [9] Whitlock, S., Gerritsma, R., Fernholz, T. & Spreuw, R. J. C. Two-dimensional array of microtraps with atomic shift register on a chip. *New J. Phys.* **11**, 023021 (2009).
 - [10] Møller, D., Madsen, L. B. & Mølmer, K. Quantum Gates and Multiparticle Entanglement by Rydberg Excitation Blockade and Adiabatic Passage. *Phys. Rev. Lett.* **100**, 170504 (2008).
 - [11] Müller, M., Lesanovsky, I., Weimer, H., Büchler, H. P. & Zoller, P. Mesoscopic Rydberg gate based on electromagnetically induced transparency. *Phys. Rev. Lett.* **102**, 170502 (2009).
 - [12] Gaëtan, A. *et al.* Observation of collective excitation of two individual atoms in the Rydberg blockade regime. *Nature Phys.* **5**, 115–118 (2009).
 - [13] Urban, E. *et al.* Observation of Rydberg blockade between two atoms. *Nature Phys.* **5**, 110–114 (2009).
 - [14] Breuer, H.-P. & Petruccione, F. *The Theory of Open Quantum Systems* (Oxford University Press, Oxford, 2002).
 - [15] Feynman, R. P. Simulating physics with computers. *Int. J. Theo. Phys.* **21**, 467–488 (1982).
 - [16] Lloyd, S. Universal Quantum Simulators. *Science* **273**, 1073–1078 (1996).
 - [17] Kitaev, A. Y. Fault-tolerant quantum computation by anyons. *Ann. Phys.* **303**, 2–30 (2003).
 - [18] S. Diehl *et al.* Quantum states and phases in driven open quantum systems with cold atoms. *Nature Phys.* **4**, 878–

- 883 (2008).
- [19] Kraus, B. *et al.* Preparation of entangled states by quantum Markov processes. *Phys. Rev. A* **78**, 042307 (2008).
- [20] Aguado, M., Brennen, G. K., Verstraete, F. & Cirac, J. I. Creation, Manipulation, and Detection of Abelian and Non-Abelian Anyons in Optical Lattices. *Phys. Rev. Lett.* **101**, 260501 (2008).
- [21] Bombin, H. & Martin-Delgado, M. A. Topological Quantum Distillation. *Phys. Rev. Lett.* **97**, 180501 (2006).
- [22] Kitaev, A. Y. Anyons in an exactly solved model and beyond. *Ann. Phys.* **321**, 2–111 (2006).
- [23] Duan, L.-M., Demler, E. & Lukin, M. D. Controlling Spin Exchange Interactions of Ultracold Atoms in Optical Lattices. *Phys. Rev. Lett.* **91**, 090402 (2003).
- [24] Jackeli, G. & Khaliullin, G. Mott Insulators in the Strong Spin-Orbit Coupling Limit: From Heisenberg to a Quantum Compass and Kitaev Models. *Phys. Rev. Lett.* **102**, 017205 (2009).
- [25] Sørensen, A. & Mølmer, K. Spin-Spin Interaction and Spin Squeezing in an Optical Lattice. *Phys. Rev. Lett.* **83**, 2274–2277 (1999).
- [26] Bloch, I., Dalibard, J. & Zwerger, W. Many-body physics with ultracold gases. *Rev. Mod. Phys.* **80**, 885–964 (2008).
- [27] Vidal, J., Dusuel, S. & Schmidt, K. P. Low-energy effective theory of the toric code model in a parallel magnetic field. *Phys. Rev. B* **79**, 033109 (2009).
- [28] Fölling, S. *et al.* Spatial quantum noise interferometry in expanding ultracold atom clouds. *Nature* **434**, 481–484 (2005).
- [29] Altman, E., Demler, E. & Lukin, M. D. Probing many-body states of ultracold atoms via noise correlations. *Phys. Rev. A* **70**, 013603 (2004).
- [30] Kogut, J. B. An introduction to lattice gauge theory and spin systems. *Rev. Mod. Phys.* **51**, 659–713 (1979).
- [31] Moessner, R. & Sondhi, S. L. Resonating Valence Bond Phase in the Triangular Lattice Quantum Dimer Model. *Phys. Rev. Lett.* **86**, 1881–1884 (2001).
- [32] Motrunich, O. & Senthil, T. Exotic order in simple models of bosonic systems. *Phys. Rev. Lett.* **89**, 277004 (2002).
- [33] Hermele, M., Fisher, M. P. A. & Balents, L. Pyrochlore photons: The $U(1)$ spin liquid in a $S = 1/2$ three-dimensional frustrated magnet. *Phys. Rev. B* **69**, 064404 (2004).
- [34] Levin, M. & Wen, X.-G. Colloquium: Photons and electrons as emergent phenomena. *Rev. Mod. Phys.* **77**, 871–879 (2005).
- [35] Rokhsar, D. & Kivelson, S. Superconductivity and the Quantum Hard-Core Dimer Gas. *Phys. Rev. Lett.* **61**, 2376–2379 (1988).
- [36] Fleischhauer, M., Imamoglu, A. & Marangos, J. P. Electromagnetically induced transparency: Optics in coherent media. *Rev. Mod. Phys.* **77**, 633–673 (2005).
- [37] Stokes, K. D. *et al.* Precision position measurement of moving atoms using optical fields. *Phys. Rev. Lett.* **67**, 1997–2000 (1991).
- [38] Gorshkov, A. V., Jiang, L., Greiner, M., Zoller, P. & Lukin, M. D. Coherent Quantum Optical Control with Subwavelength Resolution. *Phys. Rev. Lett.* **100**, 093005 (2008).
- [39] Li, W., Tanner, P. J. & Gallagher, T. F. Dipole-Dipole Excitation and Ionization in an Ultracold Gas of Rydberg Atoms. *Phys. Rev. Lett.* **94**, 173001 (2005).
- [40] Walker, T. G. & Saffman, M. Consequences of Zeeman degeneracy for the van der Waals blockade between Rydberg atoms. *Phys. Rev. A* **77**, 032723 (2008).

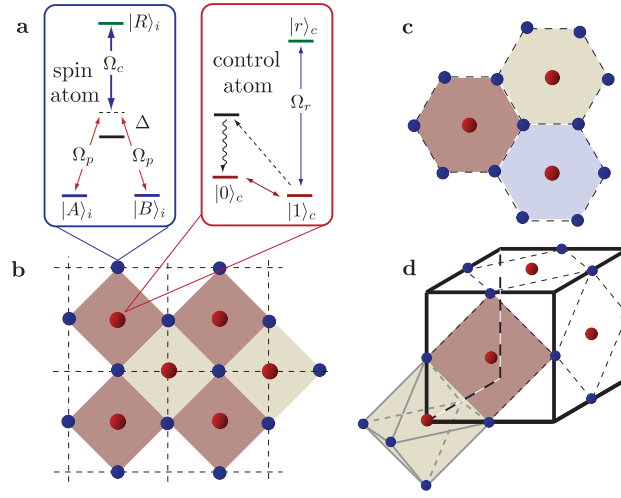


Figure 1: Setup of the system: a) Two internal states $|A\rangle_i$ and $|B\rangle_i$ give rise to an effective spin degree of freedom. These states are coupled to a Rydberg state $|R\rangle_i$ in two-photon resonance, establishing an EIT condition. On the other hand, the control atom has two internal states $|0\rangle_c$ and $|1\rangle_c$. The state $|1\rangle_c$ can be coherently excited to a Rydberg state $|r\rangle_c$ with Rabi frequency Ω_r , and can be optically pumped into the state $|0\rangle_c$ for initializing the control qubit. b) For the toric code, the system atoms are located on the links of a 2D square lattice, with the control qubits in the centre of each plaquette for the interaction A_p and on the sites of the lattice for the interaction B_s . Setup required for the implementation of the color code (c), and the $U(1)$ lattice gauge theory (d).

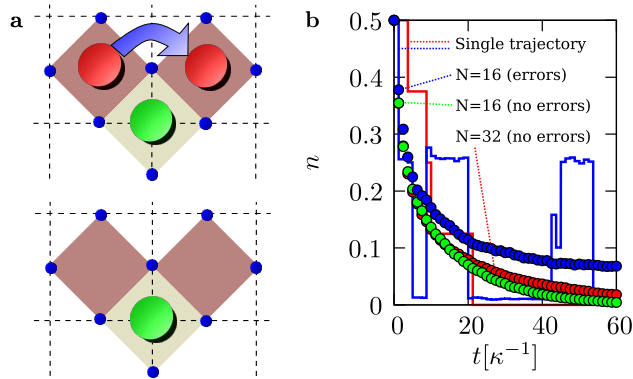


Figure 2: Cooling of the toric code: a) A dissipative time step moves one anyonic excitation (red dot) on top of a second anyon sitting on a neighboring plaquette, annihilating each other and thus lowering the internal energy of the system. The anyon of different type (green dot) is unaffected as moves of anyons occur only with a small probability. b) Numerical simulation of the cooling for N lattice sites (periodic boundary conditions). Single trajectories for the anyon density n over time are shown as solid lines. Filled circles represent averages over 1000 trajectories. The initial state for the simulations is the fully polarized, experimentally easily accessible state of all spins down. For perfect gates the energy of the system reaches the ground state energy in the long time limit, while for imperfect gates heating events can occur (blue solid line) and a finite density of anyons n remains present (blue circles). In this example the phase shift determining the cooling rate was set to $\theta = 1.25$ providing a characteristic time scale $\kappa^{-1} \sim 8\mu\text{s}$, while the parameter quantifying the gate error was $|Q| = 0.1$ (see the Methods section for details).

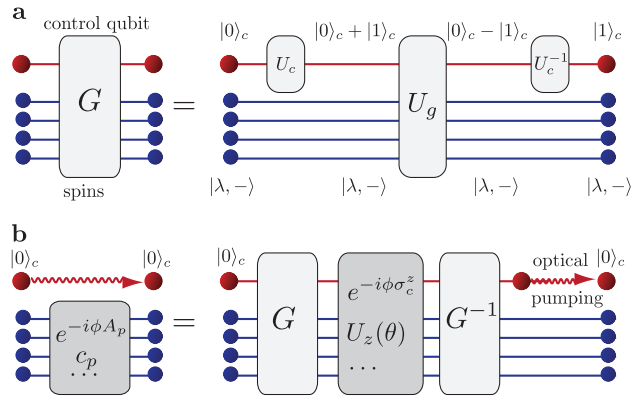


Figure 3: Single time step: a) The gate sequence G coherently maps the information, whether the system spins reside in any eigenstate $|\lambda, -\rangle$ ($|\lambda, +\rangle$) corresponding to the eigenvalue -1 ($+1$) of the many-body interaction A_p onto the internal state $|1\rangle_c$ ($|0\rangle_c$) of the control qubit. b) After the mapping G , we apply gate operations, which depend on the internal state of the control qubit. Finally, the mapping G is reversed and the control qubit is incoherently reinitialized in state $|0\rangle_c$ by optical pumping. At the end of the complete sequence the dynamics of the control qubit factors out.

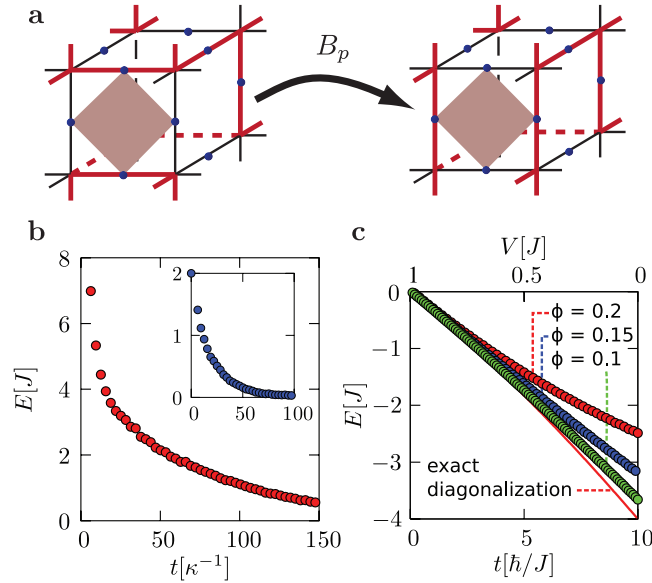


Figure 4: Lattice gauge theory: a) Illustration of a dimer covering with three dimers (red links) meeting at each site of the cubic lattice. The front plaquette represents a flipable plaquette, which is transformed under the action of the ring-exchange B_p into a different dimer covering. b) Numerical simulation for the cooling into the ground state at the Rokhsar-Kivelson point with $E = 0$ for a system with 4 unit cells (12 spins). The cooling into the constraint on the octahedra follows in analogy to the cooling of the toric code via the diffusion and annihilation of 'electric charges' on the octahedra. The inset shows the cooling into the equal superposition of all dimer coverings starting from an initial state satisfying the constraint on all octahedra. c) Coherent time evolution from the Rokhsar-Kivelson point with a linear ramp of the Rokhsar-Kivelson term $V(t) = J(1 - tJ/10\hbar)$: the solid line denotes the exact ground state energy, while the dots represent the digital time evolution during an adiabatic ramp for different phases ϕ written during each time step. The difference accounts for errors induced by the Trotter expansion due to the non-commutative terms in the Hamiltonian.